PRIMARY RESEARCH ARTICLE

Global Change Biology WILEY

Modelling past and future peatland carbon dynamics across the pan-Arctic

Nitin Chaudhary[1] (iD) | Sebastian Westermann[1] | Shubhangi Lamba[2] | Narasinha Shurpali[3] (iD) | A. Britta K. Sannel[4] | Guy Schurgers[5] | Paul A. Miller[6] | Benjamin Smith[6]

[1]Department of Geosciences, University of Oslo, Oslo, Norway

[2]Department of Biological and Environmental Sciences, University of Gothenburg, Gothenburg, Sweden

[3]Department of Environmental and Biological Sciences, University of Eastern Finland, Kuopio, Finland

[4]Department of Physical Geography, Stockholm University, Stockholm, Sweden

[5]Center for Permafrost (CENPERM), Department of Geosciences and Natural Resource Management, University of Copenhagen, Copenhagen, Denmark

[6]Department of Physical Geography and Ecosystem Science, Lund University, Lund, Sweden

Correspondence
Nitin Chaudhary, Department of Geosciences, University of Oslo, Sem Sælands vei 1, Geologibygningen, 0371 Oslo, Norway.
Email: nitin.chaudhary@geo.uio.no or nitin.chj@gmail.com

Abstract

The majority of northern peatlands were initiated during the Holocene. Owing to their mass imbalance, they have sequestered huge amounts of carbon in terrestrial ecosystems. Although recent syntheses have filled some knowledge gaps, the extent and remoteness of many peatlands pose challenges to developing reliable regional carbon accumulation estimates from observations. In this work, we employed an individual- and patch-based dynamic global vegetation model (LPJ-GUESS) with peatland and permafrost functionality to quantify long-term carbon accumulation rates in northern peatlands and to assess the effects of historical and projected future climate change on peatland carbon balance. We combined published datasets of peat basal age to form an up-to-date peat inception surface for the pan-Arctic region which we then used to constrain the model. We divided our analysis into two parts, with a focus both on the carbon accumulation changes detected within the observed peatland boundary and at pan-Arctic scale under two contrasting warming scenarios (representative concentration pathway—RCP8.5 and RCP2.6). We found that peatlands continue to act as carbon sinks under both warming scenarios, but their sink capacity will be substantially reduced under the high-warming (RCP8.5) scenario after 2050. Areas where peat production was initially hampered by permafrost and low productivity were found to accumulate more carbon because of the initial warming and moisture-rich environment due to permafrost thaw, higher precipitation and elevated CO_2 levels. On the other hand, we project that areas which will experience reduced precipitation rates and those without permafrost will lose more carbon in the near future, particularly peatlands located in the European region and between 45 and 55°N latitude. Overall, we found that rapid global warming could reduce the carbon sink capacity of the northern peatlands in the coming decades.

KEYWORDS
basal age, carbon accumulation, climate change, dynamic global vegetation models (DGVMs), peatland, permafrost

1 | INTRODUCTION

Peatlands are important terrestrial ecosystems owing to their large carbon (C) reserve (MacDonald et al., 2006). According to recent estimates, around 400–500 Pg [10^{15} g] C have been sequestered in these ecosystems since the beginning of the Holocene (Gorham, 1991; Yu, Loisel, Brosseau, Beilman, & Hunt, 2010). However, the distribution of peat soil organic C is uneven and widespread across the pan-Arctic region (45–75°N; Kleinen, Brovkin, & Schuldt, 2012; Loisel et al., 2014; Xu, Morris, Liu, & Holden, 2018). There is still some uncertainty surrounding both the distribution of the peatland area and total C storage so that the estimated C budget remains speculative (Yu, Beilman, & Jones, 2009). This uncertainty mainly stems from limited and sporadic spatial and temporal estimates of C accumulation rates (CARs; Loisel et al., 2014). The extent and remoteness of the northern domain pose a challenge to developing reliable regional C accumulation estimates. Recent syntheses have filled some of these knowledge gaps, but many regions are yet to be explored (Loisel et al., 2014; Yu et al., 2009). Modelling studies are useful in the present context, as many state-of-the-art models (see table S1 in Chaudhary, Miller, & Smith, 2017a) have now included peatland and permafrost processes in their framework. Simulation tools can therefore predict reasonable CARs at many peatland sites, making them reliable tools for reducing CAR uncertainties at different spatial and temporal scales (Alexandrov, Brovkin, & Kleinen, 2016; Chaudhary, Miller, & Smith, 2017b; Wu, Verseghy, & Melton, 2016). However, these recent modelling attempts have also indicated that the models will require reliable climate forcing data for realistic predictions of CARs. In particular, models must have a proper representation of freezing–thawing processes in cold regions and need to be constrained with correct peat basal ages (Chaudhary et al., 2017b).

A large fraction of northern latitude land areas is underlain by permafrost (Obu et al., 2019). In areas without glacial ice cover, permafrost started developing in the Pleistocene period—such areas hold the thickest permafrost today (French, 1999). On the other hand, a significant part of today's permafrost extent was formed after deglaciation of the Laurentide and Fennoscandian ice sheets. A substantial area of northern peatlands coincides with low altitude permafrost areas of both Pleistocene and Holocene origin (Hugelius et al., 2014; Wania, Ross, & Prentice, 2009). Globally, permafrost peatlands store around 277–302 Pg C which is equivalent to about 14% of the global soil C (Hugelius et al., 2014). Permafrost has an intricate and complex relationship with peatland vegetation, hydrology and biogeochemistry (Vardy, Warner, Turunen, & Aravena, 2000). Peat deposits in combination with permafrost lead to distinct landforms, such as palsas, peat plateaus and polygonal peat plateaus with shallow active layer depths (Malmer, Johansson, Olsrud, & Christensen, 2005). Being strongly coupled with all the major biogeochemical components of peatlands, alterations in the present state of permafrost can have severe implications for the overall peatland carbon balance (Robinson & Moore, 2000).

Peat basal ages provide an understanding of peatland initiation (Yu, 2012) and thus indirectly shed light on associated deglaciation processes and past changes in climate (Chambers et al., 2012), with wet and moderately warm conditions typically leading to the initiation of new peatlands. Databases of basal radiocarbon ages from peatlands show regional differences in the timing of peatland initiation (Loisel et al., 2014; Yu et al., 2010). It is believed that there is no specific factor which is solely responsible for peatland initiation and its further development, but rather a combination of several factors, such as geomorphology, local hydrology, climate, moisture conditions, substrate, bedrock composition and permafrost, among others (Korhola et al., 2010; Kuhry & Turunen, 2006; Morris et al., 2018; Ruppel, Valiranta, Virtanen, & Korhola, 2013; Weckstrom, Seppa, & Korhola, 2010). Predicting accurate basal age through modelling is therefore challenging. Since the majority of peatlands formed between 8,000 and 10,000 calendar years before present (ky cal. BP) in northern regions (Yu et al., 2010), modelling studies (Chaudhary et al., 2017a; 2017b) typically use a fixed indicative period during the model initialization stage, for example, 10 ky cal. BP. However, this simplified strategy ignores the effects of many important factors such as ice sheet cover and post-glacial rebound, local climate, substrate, topography and other unknown factors which may have triggered and influenced peat formation or caused a lag in peatland development (MacDonald et al., 2006; Yu et al., 2010) at different locations, resulting in spatiotemporally variable CARs. In the absence of reliable parametrizations for peatland initiation, models must be prescribed with correct peat basal ages for reliable predictions to minimize uncertainty related to the timing of peatland formation.

Dynamic global vegetation models (DGVMs) are used to study changes in vegetation patterns at different spatial and temporal scales together with associated biogeochemical and climate feedbacks (Cramer et al., 2001; Friedlingstein et al., 2006; Sitch et al., 2008; Strandberg et al., 2014; Zhang, Jansson, Miller, Smith, & Samuelsson, 2014). Currently, a handful of vegetation models feature a representation of both peatland and permafrost ecosystems which is a prerequisite to quantify peatland carbon dynamics in past, present and future climates (Kleinen et al., 2012; Stocker, Spahni, & Joos, 2014; Wania et al., 2009). Formulations of multiple peat-layers accumulation and decay have been demonstrated at the site scale (Bauer, 2004; Frolking et al., 2010; Heinemeyer et al., 2010) and recently been integrated in the framework of DGVMs for large area application (Chaudhary et al., 2017a). Peatland processes have also been incorporated in other modelling frameworks, performing reasonably well for peatland sites (Alexandrov et al., 2016; Morris, Baird, & Belyea, 2012; Wu et al., 2016). A number of models have performed large area simulations to account for regional peatland carbon dynamics (e.g. Alexandrov et al., 2016; Kleinen et al., 2012; Qiu et al., 2019; Schuldt, Brovkin, Kleinen, & Winderlich, 2013; Stocker et al., 2014; see supplementary table S1 and para 2, p. 2571 in Chaudhary et al., 2017a for more details).

Earlier studies (Chaudhary et al., 2017a; 2017b) have shown that the uncertainty in predicting CAR can be minimized if the models are constrained with correct peat initiation time. In this work, three

different published datasets of peat basal ages (Gorham, Lehman, Dyke, Janssens, & Dyke, 2007; Korhola et al., 2010; MacDonald et al., 2006), supplemented by independent measurements (Chaudhary et al., 2017a; Loisel et al., 2014; Yu et al., 2009), have been combined to a peat inception map for the pan-Arctic region. Initiate model simulations with this peat inception map, we employ the individual- and patch-based dynamic global ecosystem model—LPJ-GUESS (Smith, Prentice, & Sykes, 2001) with dynamic peatland and permafrost functionality (Chaudhary et al., 2017a) to quantify CARs at different temporal scales across the pan-Arctic region. The model accounts for the close coupling between peatland, permafrost and vegetation dynamics which is critical for the formation and evolution of these C-rich ecosystems. We analyse the influence of historical climate change on peatland C balance, CARs and permafrost distribution at regional scale, and compare to corresponding simulated values for future climate change scenarios (representative concentration pathway—RCP2.6 and RCP8.5).

2 | MATERIALS AND METHODS

2.1 | Model description

LPJ-GUESS (Lund–Potsdam–Jena General Ecosystem Simulator) is a process-based, dynamic, second-generation model of vegetation dynamics, plant physiology and the biogeochemistry of terrestrial ecosystems (Smith et al., 2001, 2014). It simulates a dynamic vegetation structure and composition in response to changing climate conditions and is optimized for regional to global applications. Plant demography and community structure evolve in replicate patches subject to the stochastic establishment, mortality and disturbance, forced by climate, CO_2 and hydrological inputs altering the biogeophysical and biogeochemical characteristics of terrestrial ecosystems. The model has been evaluated against a number of observational datasets and other models (see e.g. Ekici et al., 2015; McGuire et al., 2012; Piao et al., 2013).

We employed a customized version of LPJ-GUESS for Arctic applications which includes dynamic peat accumulation and decomposition functionality in conjunction with permafrost/freeze–thaw cycle (Chaudhary et al., 2017a). Peat accumulation is a product of annual litter input and decomposition losses: The peat is composed of a fraction of the dead litter C mass derived from roots, leaves, seeds and stems. The dead litter, which is a product of mortality, productivity and leaf and root turnover specific to plant functional types (PFTs), is initially deposited on top of a static mineral surface. The dead litter is treated as a peat mass which decomposes based on the initial decomposition rate, the quality of litter, and the soil thermal and hydrological properties in each layer within an individual patch. The decomposition is computed on a daily time step, and the peat's intrinsic properties and structure are parameterized by an initial decomposition rate (k_o) which declines over time (Aerts, Verhoeven, & Whigham, 1999; Chaudhary et al., 2017b; Frolking et al., 2001). The peatland hydrology is simulated using a simple

bucket scheme where precipitation and snow melt are assumed to fill the bucket and evapotranspiration, drainage and base run-off remove water (Gerten, Schaphoff, Haberlandt, Lucht, & Sitch, 2004). We simulate water and ice in each peat layer of individual patch and convert them to water and ice content by dividing the amount of ice and water with total water holding capacity. If a layer is completely frozen (100% ice), it cannot hold additional water. In partially frozen soil, the sum of the fractions of water and ice is limited to the water holding capacity of that layer. The soil water content determines the peat decomposition rate in individual layers. We calculate the landscape water table position (WTP) and add and remove the amount of water from each patch required to match the landscape mean WTP.

In the current setup, multiple vegetation patches are simulated that account for the spatial heterogeneity within a peat-bearing landscape. In the model, the vegetation is represented as a mixture of PFTs, that is collections of species with similar functional and morphological characteristics. The peatland vegetation in LPJ-GUESS is represented by five PFTs: graminoids (Gr), mosses (M), high summergreen shrubs (HSS), low summergreen shrubs (LSS) and low evergreen shrubs (LSE). The model is initialized with a random surface represented by uneven heights of individual patches (10 in the simulations performed here). At the end of each simulation year, the water is redistributed from the higher elevated sites to low depressions by means of lateral flow. We equalize the WTP of individual patches according to the mean WTP of the landscape. The higher patches lose water if their WTP is above the mean WTP of the landscape, while the patches with a WTP below the mean receive water. This, in turn, affects the plant productivity and decomposition rate in each patch, which further modifies the surface conditions. Shrubs dominate in dry conditions with WTPs below −25 cm (negative signs signify a WTP below the peat surface), while mosses and graminoids are favoured by comparatively saturated conditions: graminoids favour inundated conditions (WTP is above +10 cm) and mosses establish for WTPs between −50 and +5 cm. The establishment function is implemented annually based on annual mean WTP. The different PFTs feature specific physiological, morphological and life-history characteristics governing their interactions and response to climate. Carbon allocation, phenology, rooting depth, tolerance for waterlogging and decomposability of plant litter are key PFT parameters, in conjunction with prescribed bioclimatic limits and average WTP determining their growth and distribution (Chaudhary et al., 2017b; Miller & Smith, 2012). The full parameter sets for these PFTs are given in Miller and Smith (2012) and Chaudhary et al. (2017b) and a detailed description of the model can be found in Chaudhary et al. (2017a).

2.2 | Simulation protocol and data requirement

#### 2.2.1 | Hindcast experiment

To achieve a better spatial and temporal understanding of the Holocene peatland development and C dynamics across the

pan-Arctic region, the model was run for 969 randomly selected grid points (referred to as 'sites' below) distributed across the northern latitude domain (45–75°N; Figure 1a), of which 287 fall within the observed peatland boundary (Xu et al., 2018; see Figure 1a,b). In the following, we refer to this subset of 287 points as the 'mapped peatland ensemble', while the full ensemble of 969 points is referred to as the 'pan-Arctic all peat scenario'. The model results for the 'mapped peatland ensemble' represent the best guess considering the presently known peatland extent, while the 'pan-arctic all peat scenario' constitutes a hypothetic upper bound taking potentially unmapped peatlands into account (resulting values presented in brackets; see Table 1).

To reach an approximate equilibrium of vegetation and C pools with respect to early climate conditions, the model was initialized for each site for 500 years from 'bare ground' using the first 30 years of historical climate forcing data (explained below). The mineral and peat layers were forced to remain saturated for the entire initialization period. The peat decomposition, soil temperature and water balance calculations were not started until the peat column became sufficiently thick (0.5 m). This initialization strategy was adopted to avoid a sudden collapse of the peat column in very dry spells due

to feedbacks between temperature-dependent peat decomposition and thus reduced water holding capacity. The shallow peat layers in the low-latitude regions are highly susceptible to these anomalies affecting the peat dynamics and CAR.

To take the observed peatland initiation period into account for each modelled cell, we first extracted and combined approximately 5,000 peat basal points (see Figure 1c) from three published datasets (Gorham et al., 2007; Korhola et al., 2010; MacDonald et al., 2006). Additional peat basal points were also added from other sources (Chaudhary et al., 2017a; Yu et al., 2009). We identified and removed identical points and retained the oldest basal age. The filtered basal point ages (2,873 points) were then interpolated using an inverse distance weighting interpolation to generate a most up-to-date peat basal age distribution surface to constrain the model. This strategy overcomes the major uncertainty related to the peat initiation period, which is influenced by various local factors and therefore difficult to simulate at the resolution of the climate forcing data (see below). The basal age points have not been screened by the strict Reyes and Cooke (2011) protocol, which may have led to potential random errors in the peat basal age map. This means that in some places the basal age does not represent the actual peat initiation time leading to different CARs
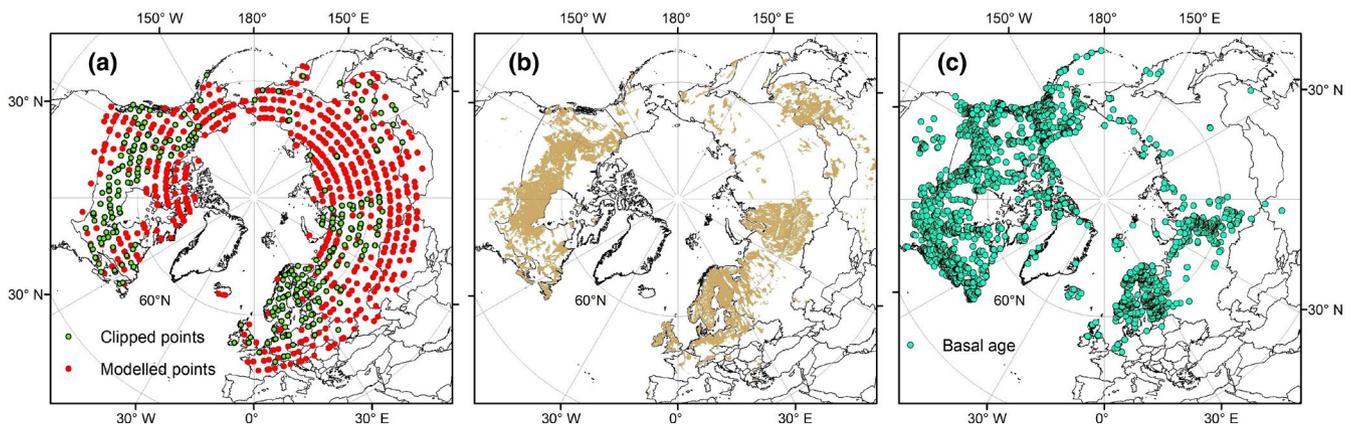
FIGURE 1 (a) Map of the pan-Arctic domain (45–75°N) showing 969 randomly selected modelled sites ('pan-Arctic all peat scenario') and the subset of 287 sites ('mapped peatland ensemble', in green) based on (b) the observed peatland boundary (Xu et al., 2018); (c) locations with observed peat basal age (2,573 points) extracted from published datasets (Gorham et al., 2007; Korhola et al., 2010; MacDonald et al., 2006)

TABLE 1 Mean carbon accumulation rates (g C m^{-2} year^{-1}) for the observed boundary and pan-Arctic scale at different time intervals

	Time interval							
			Centennial			Decadal		
Domain	Holocene	Millennium (1000–2000)	Historical (1901–2000)	Exp26 (2001–2100)	Exp85 (2001–2100)	Historical (1991–2000)	Exp26 (2091–2100)	Exp85 (2091–2100)
Mapped peatland ensemble (287 points)	21.4	17.8	24.3	29.8	25	33.1	22	5.8
Pan-Arctic all peat scenario (969 points)	23.6	21.4	27.6	27.6	24.2	33.9	20.5	10.3

(see Figure 1b,c). To drive the model, we have developed three distinct climate forcing periods: Each simulation was run from the time of peat initiation based on corresponding interpolated basal age values until the year 1900. Thereafter, a transient run was performed from the year 1900 to 2000, followed by two different future experiments for the next 100 years (2001–2100) under two different climate change scenarios.

2.2.2 | Historical climate forcing

In the first phase, we forced the model with climate fields (temperature, precipitation and cloudiness) constructed by interpolating between monthly values from the year of peat initiation (based on the prescribed basal age, see above) until the year 1900. The delta-change method, that is applying relative anomalies in temperature and precipitation, was used to form the monthly climate forcing series. Climate anomaly data were derived for the nearest global climate model grid cell to the modelled site location from the Hadley Centre's Unified Model (UM; Miller et al., 2008) and linearly interpolated values from these climate anomalies were applied to the average monthly Climatic Research Unit gridded Time Series 3.0 gridded climate dataset (Mitchell & Jones, 2005) from the period 1901 to 1930. This method conserves the inter-annual variability of temperature and precipitation from the baseline historical climate (1901–1930) throughout the simulation. The version of the UM used in this study was HadSM3, an atmospheric general circulation model coupled to simple mixed-layer ocean and sea ice models with 2.5° × 3.75° spatial resolution (Pope, Gallani, Rowntree, & Stratton, 2000). The monthly Holocene temperature values were interpolated to daily values, and monthly precipitation totals were distributed randomly among the rainy days per month (minimum 10) from the climate dataset. The monthly CRU values of cloudiness for the first 30 years from the year 1901 to 1930 were repeated for the entire simulation period. Finally, we added the variability to daily climate values by generating random values from a normal distribution with monthly mean (μ) and standard deviation (σ) of the monthly CRU values from 1901 to 1930. The second historical phase extended from 1900 to 2000 AD for which we used the CRU dataset (Mitchell & Jones, 2005) to force the model. Past atmospheric CO_2 concentrations until 1850 AD were obtained from the boundary conditions in the UM time slice experiments (Miller et al., 2008). The CO_2 concentrations used to force the UM simulations were linearly interpolated to an annually varying value between prescribed averages for each millennium (from the start of the peat initiation to 1850 AD). From the year 1850 to 2000, observed annual CO_2 from atmospheric or ice core measurements were used (McGuire et al., 2012). The model simulated higher CAR during the initial 500 years as we limit the peat decomposition until it reaches a height of 0.5 m. These anomalies were also present in our earlier studies (Chaudhary et al., 2017a; 2017b), which demanded a different strategy to avoid higher CAR due to initial peat build up. In this study, we replaced the initial

500 years with an average of the following 500 years for each site in our analysis.

2.2.3 | Climate change experiments and forcing

To investigate the sensitivity of CAR to the widest possible ranges of climate change scenarios, we performed future experiments using the RCP2.6 and RCP8.5 (Moss et al., 2010) 21st-century climate change projections (referred to as 'Exp26' and 'Exp85' in the following), extending the base experiment ('Bas') from the year 2001 to 2100. Climate output from the Coupled Model Intercomparison Project Phase 5 (CMIP5) runs with the Hadley Global Environment Model 2 (HadGEM2-ES; Collins et al., 2011) was used to provide future climate forcing. The anomalies extracted from the Exp26 and Exp85 experiments were applied to the historical CRU data to create climate forcing fields for each site. Atmospheric CO_2 concentrations for both emission scenarios were obtained from the website of the International Institute for Applied Systems Analysis (IIASA)—http://tntcat.iiasa.ac.at/RcpDb/.

2.3 | Model evaluation

To evaluate our model, observed CARs based on 127 sites (Loisel et al., 2014) were compared to modelled CARs since the beginning of the Holocene. A recently developed PEATMAP dataset (Xu et al., 2018) was combined and aggregated to generate the most up-to-date peatland distribution map (Figure 1b) across the pan-Arctic. Peatlands that fall within a 50 km radius were aggregated in the same polygon (using the ArcGIS aggregate function). This map was used to extract and identify modelled sites within the observed peatland area to calculate mean CARs for the observed peatland zone.

3 | RESULTS

3.1 | Hindcast experiment

Peatlands started forming approximately 20 ky cal. BP during the last glacial maximum but the majority (approx. 90%) developed after the Greenlandian period (12–8 ky cal. BP), which marks the beginning of the Holocene. Until the end of Northgrippian around 4.2 ky cal. BP, almost 80% of present-day peatlands had developed (Figure 2). Around 20% of peatlands initiated during the Meghalayan period after 4.2 ky cal. BP and are considered young peatlands. According to our simulations (Figure 3), northern peatlands have sequestered C at a rate of 15–30 g C m^{-2} year^{-1} during the Holocene with a mean of 21.4 (23.6) g C m^{-2} year^{-1} (see Table 1). From Figure 3, we note that modelled CARs were highest during the mid-Holocene (around 8.5 ky cal. BP). Modelled peatlands accumulated a relatively greater amount of C during the model initialization stage as the decomposition was not started until the peat height reached 0.5 m
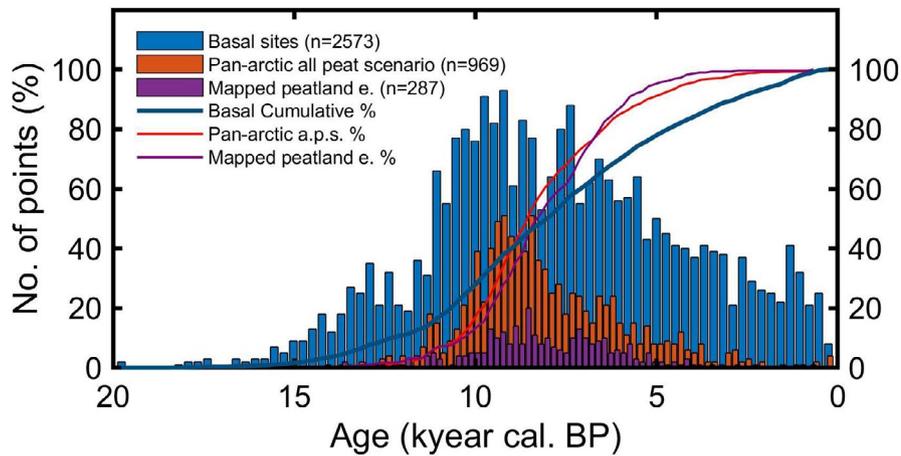
FIGURE 2 Distribution of regional peat basal age points (2,573; Gorham et al., 2007; Korhola et al., 2010; MacDonald et al., 2006) since the Last Glacial Maximum (20 ky cal. BP), including cumulative percentages; randomly selected model sites ('pan-Arctic all peat scenario', 969 points) and the subset ('mapped peatland ensemble', 287 points) within the observed peat boundary (Xu et al., 2018) are distinguished
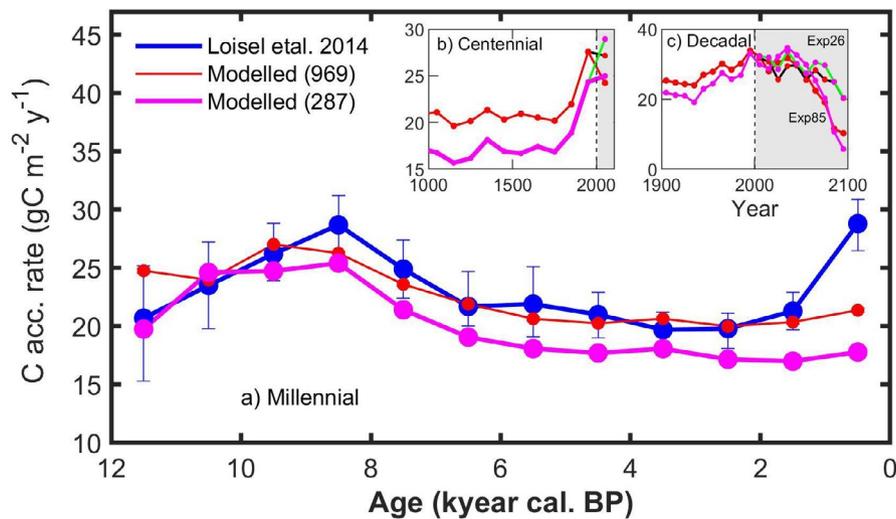

FIGURE 3 (a) Modelled (mapped peatland ensemble, 287 and pan-Arctic all peat scenario, 969) and observed mean carbon accumulation rates (CAR, in g C m^{-2} year^{-1}) for each millennium (1,000 year period) for the last 12,000 years. Red: modelled mean CAR for 'pan-Arctic all peat scenario' (r^2 = .33; root mean square error [RMSE] = 2.8). Magenta: modelled mean CAR for the 'mapped peatland ensemble', that is the points within the observed peatland boundary (r^2 = .35; RMSE = 4.1). Blue points are observed CARs (g C m^{-2} year^{-1}) based on 127 sites Loisel et al. (2014) with error bars showing the standard errors of the means, (b) modelled 'pan-Arctic all peat scenario' and 'mapped peatland ensemble' for centennial (100 year period in magenta) rates (in g C m^{-2} year^{-1}) and (c) decadal (10 year period) rates (in g C m^{-2} year^{-1}) for RCP2.6 (Exp26) with 287 ●— and 969 ●●— and RCP8.5 (Exp85) with 287 ●— and 969 ●— sites

(which is part of our initialization strategy, Section 2.2.1). Due to this artefact, higher modelled CARs can be noticed at the beginning of our simulations (Figure 3), which was partially corrected by replacing the first 500 years in each site with the average CAR of the next 500 years.

Nevertheless, the mean modelled CAR for the 'mapped peatland ensemble' is close to the observed CAR range for each 1,000 year period (Figure 3a; magenta dots with a solid magenta line), following similar temporal patterns as observations (Loisel et al., 2014; Yu et al., 2009). A sharp reduction after 8.5 ky cal. BP and a slight dip after 5 ky cal. BP can be noticed in the observed CARs. The observed rates calculated by Loisel et al. (2014) using observed CAR at 127 sites are more representative for pan-Arctic rates than the earlier observation by Yu et al. (2009). The modelled CAR for the 'pan-Arctic all peat scenario' largely follows a similar temporal trend. A sharp increase in CAR can

be noticed in the observational dataset, which is not reproduced by the modelled values at the end of the time series. However, the observational dataset includes CAR values from after 2000 AD, which partly explains the high CAR in modern times. In our analysis, only the mean of the last 1,000 years (from 1001 to 2000 AD) is considered so that the higher peat growth after 2000 AD evident from our future experiments (see Figure 4c–f, I and II) is not contained. The 'pan-Arctic all peat scenario' (969 sites) showed similar CAR variability and trends as the 'mapped peatland ensemble' (287 sites).

The CAR for the last millennium falls within the range 15–30 g C m^{-2} year^{-1} and the accumulation rates are relatively higher since the start of the industrial period (after 1850), probably due to milder climate and partial decomposition of some of the recently accumulated peat layers (Figure 3b). In the last few decades of the 20th century, the CAR reaches values of up to 30–40 g C m^{-2} year^{-1}
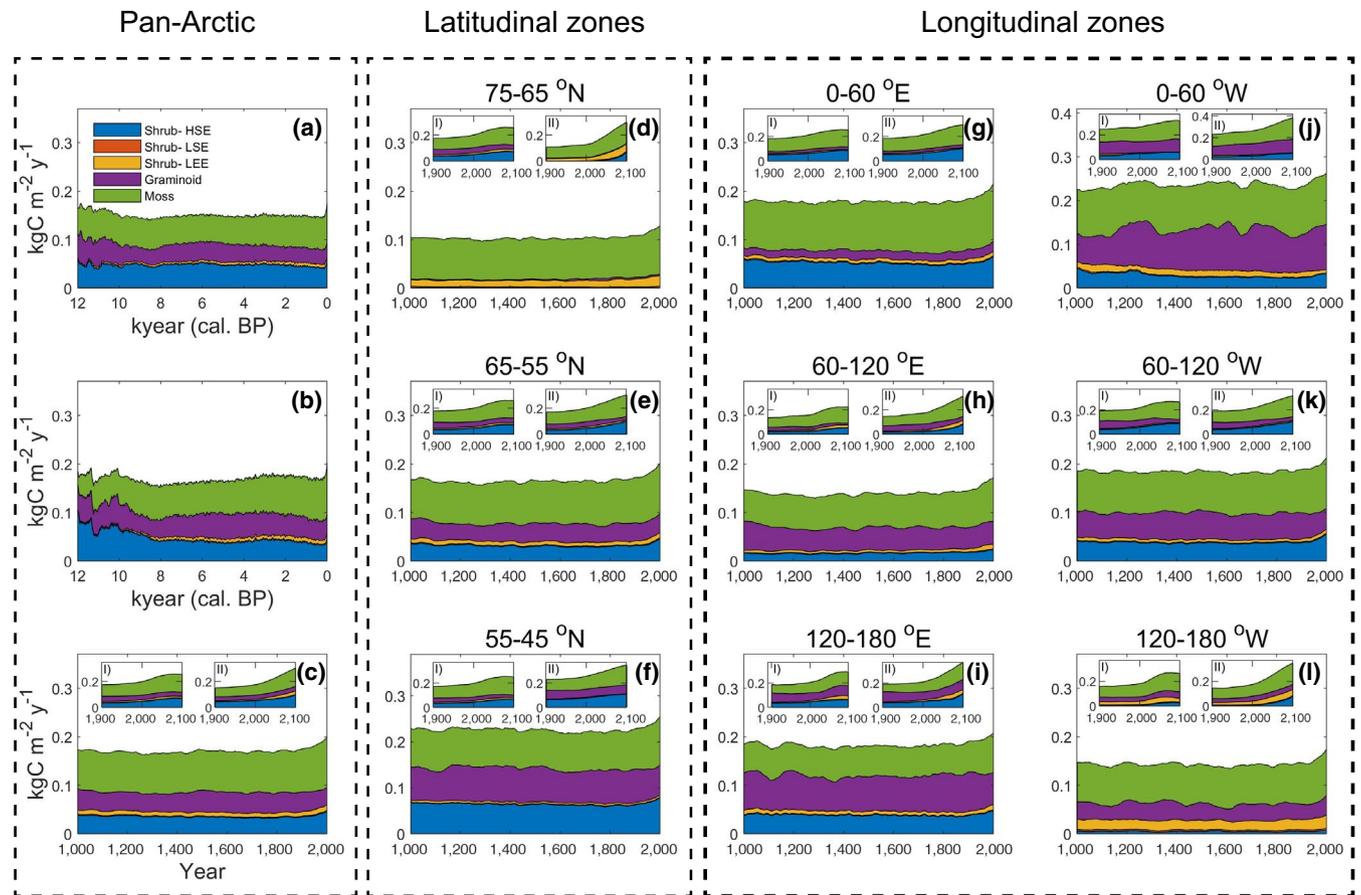
FIGURE 4 Long-term net primary productivity distributed among plant functional types for (a–c) the pan-Arctic region, using the 'pan-Arctic all peat scenario' (a) and the 'mapped peatland ensemble' (b) for the last 12,000 years (kyear) and (c) for the last millennium (1000–2000 AD); (d–f) is sorted according to different latitudinal zones from 45 to 75°N; (g–i) is sorted according to longitudinal zones from 0 to 180°E and W. Panels (i) and (ii) from (c) to (l) show the future Exp26 (left inset) and Exp85 (right inset) experiments ('mapped peatland ensemble' used for c–l)

(Figure 3c), suggesting an increasing trend in CAR. As with the early and mid-Holocene trends, the 'mapped peatland ensemble' showed similar accumulation patterns and trends for the last millennium and the 20th century compared to the 'pan-Arctic all peat scenario'.

Plant litter is derived from five plant types: M, Gr, LES, HSS and LSS, where mosses are the dominant contributor (Figures 4a–c and 5a,b). Figure 4a,b shows that the net primary productivity (NPP) for both the 'mapped peatland ensemble' and the 'pan-Arctic all peat scenario' is around 150–200 g C m⁻² year⁻¹ since the start of the Holocene. The plant productivity declines from lower (45–55°N) to higher latitude (65–75°N) areas, in conjunction with a decrease in the contribution from shrubs to NPP (Figures 4d–f and 5). In higher latitude peatlands, modelled plant litter at the end of the 20th century is mostly composed of mosses, with minor contributions from dwarf shrubs and graminoids (Figures 4d and 5a,b). Peatlands in Europe and eastern and central Canada (0–60°E and 0–120°W; Figure 4g–l) are more productive than others (Figure 4g,h), while graminoids are more productive between 0–60°W and 120–180°E due to high moisture availability in near-coastal environments (Figure 4i). Shrubs are the dominant plant type between 45 and 55°N due to high insolation and deeper WTP (Aerts et al., 1999; Pinceloup, Poulin, Brice, & Pellerin, 2020). In reality, many peatland areas are dominated by trees in such low latitudes, which is

not represented in the model employed for this study, as there are challenges in dealing with the carbon produced by trees (Chaudhary et al., 2017a). For instance, litter components such as woody debris and tree trunks represent a large carbon mass added in short time, distorting the individual peat accumulation scheme and hydrological properties. Therefore, further research is required to deal with this issue.

Permafrost formation can be classified in syngenetic and epigenetic (Ping, Jastrow, Jorgenson, Michaelson, & Shur, 2015), influencing land surface processes in different ways. Permafrost that forms at the same time as the land surface (e.g. through sedimentation or peat accumulation) is known as syngenetic permafrost, while permafrost formed in previously deposited sediments or earth material is known as epigenetic permafrost. While our model is in principle capable of simulating both permafrost formation processes, we have not isolated the influence of different permafrost formation processes on peatland development and functioning in this study. The modelled column-average September ground ice fraction in the peat soil is used as a proxy for permafrost occurrence (Figure 8a–c), as a potential active layer would generally be at its deepest thickness in September (on the N hemisphere), allowing to differentiate between permafrost and seasonally frozen ground. The modelled permafrost distribution for the recent past (averaging 1991–2000; Figure 8a) is very similar to other
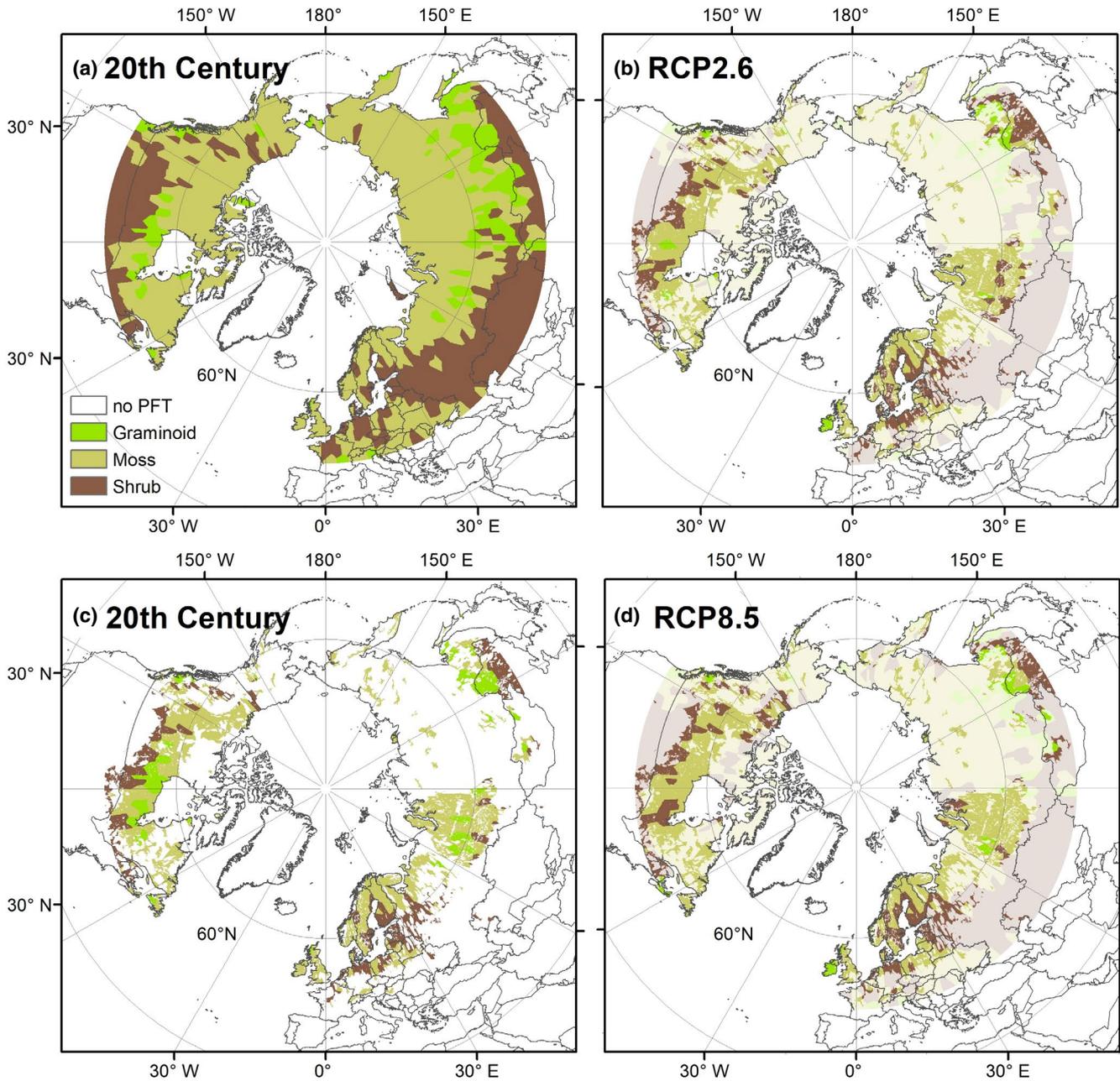
FIGURE 5 Distribution of dominant plant type across the pan-Arctic; (a) average 1991–2000; (b) clipped map according to observe peatland boundary (Xu et al., 2018); (c) under RCP2.6 (Exp26) scenario (average 2091–2100); and (d) under RCP8.5 (Exp85) scenario (average 2091–2100)

reported permafrost maps for the pan-Arctic region (for all soil types; Obu et al., 2019). Large areas in Siberia, Canada and parts of northern Scandinavia are underlain by permafrost with shallow active layer depth (0–1.5 m; Figure 8d) and the annual WTP fluctuates between −15 and 0 cm (Figure 9a,d) at the end of the 20th century in the model. Modelled areas further south featured a deeper active layer thickness, WTPs and relatively warmer climate providing suitable conditions for shrub growth (Figures 4d–f, 5a, 8a and 9a,d). The presence of permafrost does not have any direct association with peatland CAR and we find moderate to high litter accumulation (Figures 6a and 8a) in these areas. For instance, large parts of western Canada, Alaska and eastern

Siberia accumulate relatively high amounts of C (Figure 6a) by the year 2000 according to our model simulations.

3.2 | Climate change experiments

In general, modelled northern peatlands accumulated C at a rate of 10–50 g C m^{-2} year^{-1} in the recent past (averaging 1991–2000; see Figure 6a). However, there are some areas in Europe which are less productive (Figure 6a) during this period. The modelled average CAR for the same period was estimated around 33.1 (33.9 in the 'pan-Arctic
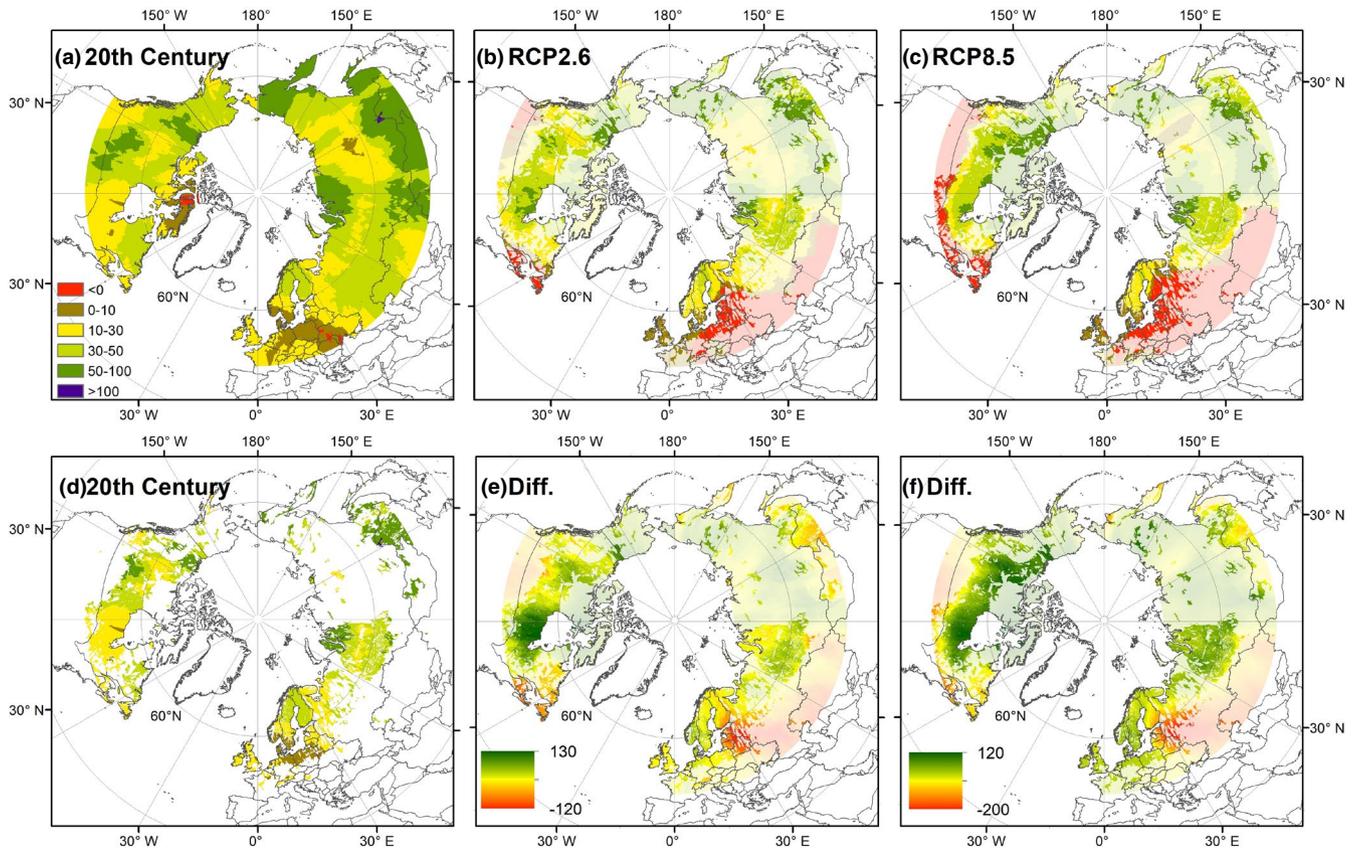
FIGURE 6 (a) Net carbon accumulation rates (in g C m^{-2} year^{-1}, average 1990–2000), (b) following the RCP2.6 scenario (Exp26; average 2091–2100), (c) following the RCP8.5 scenario (Exp85; average 2091–2100), (d) carbon accumulation rates (average 1990–2000) according to the most up-to-date observed map (PEATMAP – Xu et al. (2018), difference between RCP and present day (e) b − a; and (f) c − a

FIGURE 7 (a) Rates of peatland area change since the early Holocene according to two different estimates—3.1 and 4 million km^2 (Xu et al., 2018; Yu et al., 2010) and (b) total accumulated carbon (in Gt C) using the time-history approach
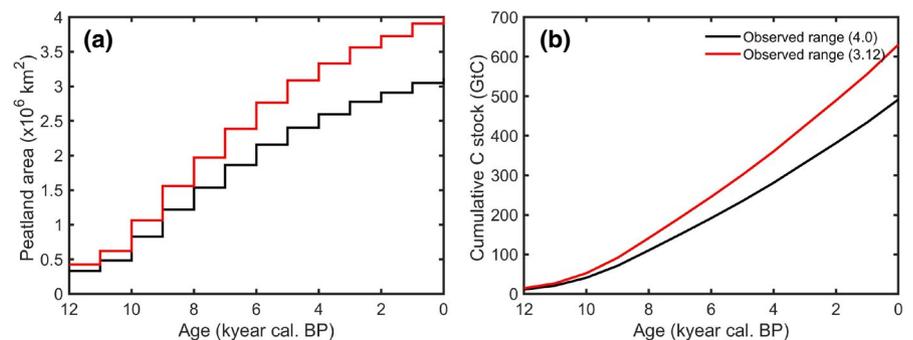
all peat scenario') which decreased to 5.8 (10.3) g C m^{-2} year^{-1} in Exp85 and 22 (20.5) in Exp26 (averaging 2091–2100; see Figures 3b,c and 6b,c and Table 1) by the end of the 21st century. The scenario simulations (see Figure 6b,c) suggest that the majority of European and western Russian peatlands, as well as low-latitude areas between 45 and 55°N, could turn into C sources by the end of the century. In contrast, our simulations indicate that northern and central Russian and Canadian peatlands might enhance their C sink capacity (Figure 6b,c,e,f). It is also clear that both C uptake intensity and C losses will increase in Exp85. However, the overall C sink capacity of peatlands could be more significantly reduced in the high-end scenario Exp85 compared to the low-emission Exp26 scenario by the end of this century.

In our analysis, the accumulation pattern and rates for the 'mapped peatland ensemble' are largely similar to the 'pan-Arctic all peat scenario' (see Figure 3b,c), emphasizing the robustness of modelled CARs. To calculate N Hemisphere C uptake by peatlands from modelled CAR, we use state-of-the-art datasets of present-day peatland extent. According to PEATMAP (Xu et al., 2018), the total peatland area across the pan-Arctic is approximately 3.1 million km^2 north of 45°N, with some studies (Yu et al., 2010) providing slightly higher estimates of up to 4 million km^2. Using both estimates with the time-history approach (Yu et al., 2010), we calculated that the northern peatlands have accumulated around 500–620 Pg C (see Figure 7) since the beginning of the Holocene.
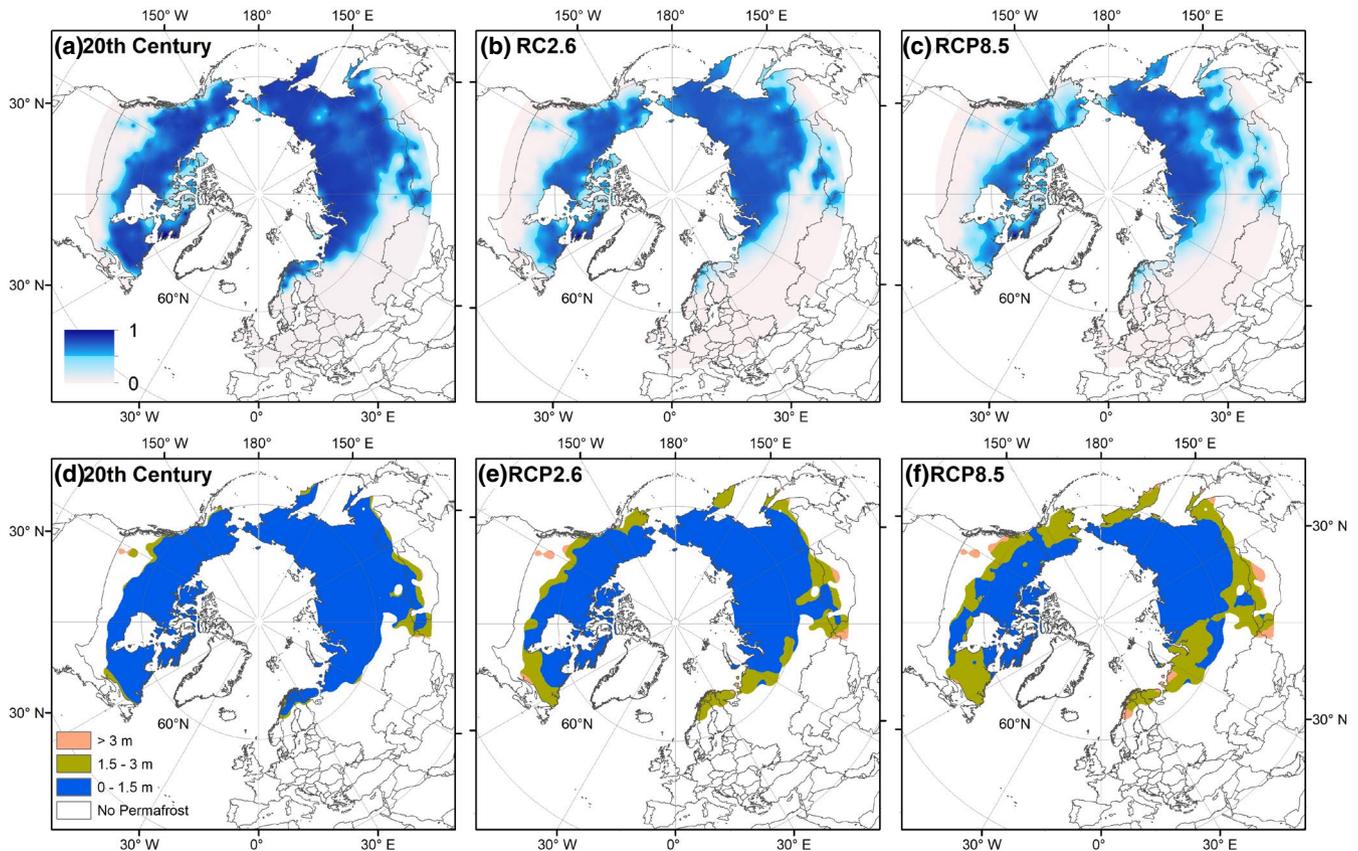
FIGURE 8 Modelled September ground ice fraction (0–1) in the peat soil (as a proxy for permafrost distribution) interpolated among modelled sites averaged over (a) 1991–2000 and (b) 2091–2100 under RCP2.6 (Exp26), and (c) under RCP8.5 (Exp85) scenarios; (d) modelled mean September active layer depth (cm) interpolated between modelled sites for 1991–2000; (e) for RCP2.6 scenario (Exp26; average 2091–2100), (f) for RCP8.5 scenario (Exp85; average 2091–2100)

We found that a large part of the Siberian region would remain a C sink under both climate change experiments, but the C sink capacity can vary greatly between these extremes (Figures 4h,i[I,II] and 6b–f). In Exp85, high C accumulation is linked to higher plant productivity and wetter soil conditions (see Figures 4h[I], 6c,f, 8c,f and 9c,f). As permafrost thaws, the active layer deepens, providing sufficient moisture for plant growth (Figures 6c,f and 8c,f). Moreover, the modelled plant productivity is further promoted by high CO_2 levels in Exp85, leading to higher CARs (Figure 4d–I[II]). On the other hand, the Exp26 experiment is associated with rather limited warming and precipitation rates, as well as moderate CO_2 increases. Here, we found that projected warming is not strong enough to degrade the underlying permafrost (Figure 8b,e) and replenish the soil moisture (Figure 9b,e). Still, the WTP deepens as evaporation rates increase, allowing woody shrubs to dominate in certain places (Figure 5c). However, C loss due to high soil decomposition rate are found to be comparatively low, since the warming is much less pronounced as in Exp85. Northern Europe, southern Canada, parts of Alaska and eastern and western parts of Siberia are projected to lose a significant amount of frozen ground leading to deeper active layer (Figure 9b–f) and wetter soil conditions, resulting in a higher plant productivity and CARs (Figure 6c,f).

In contrast, permafrost-free areas with low future rainfall experience moisture stress conditions leading to a significant C loss to the atmosphere (Figure 6c). Drier conditions also promote shrub expansion which are shown in Figures 4d–f[I,II] and 5c–d. As shrubs move northwards in response to more favourable climate conditions, the associated plant litter composition changes, forming less recalcitrant material highly susceptible to decomposition (Figure 4d–f[I–II]). We also find that the area of peatlands dominated by wet graminoids is projected to shrink significantly as WTP deepens (Figures 5c,d and 9b–f).

4 | DISCUSSION

Our simulations resulted in four estimates of peatland C balance, using two different spatial extents ('mapped peatland ensemble' and 'pan-Arctic all peat scenario') and two different warming scenarios (Exp26 and Exp85). The actual peatland distribution lies somewhere between the two spatial extents examined, but likely much closer to the state-of-the-art observational extent (i.e. the 'mapped peatland ensemble') than the theoretical upper bound of the 'pan-Arctic all peat scenario'. However, this approach provides an indication of the possible range of future peatland responses to changing climate
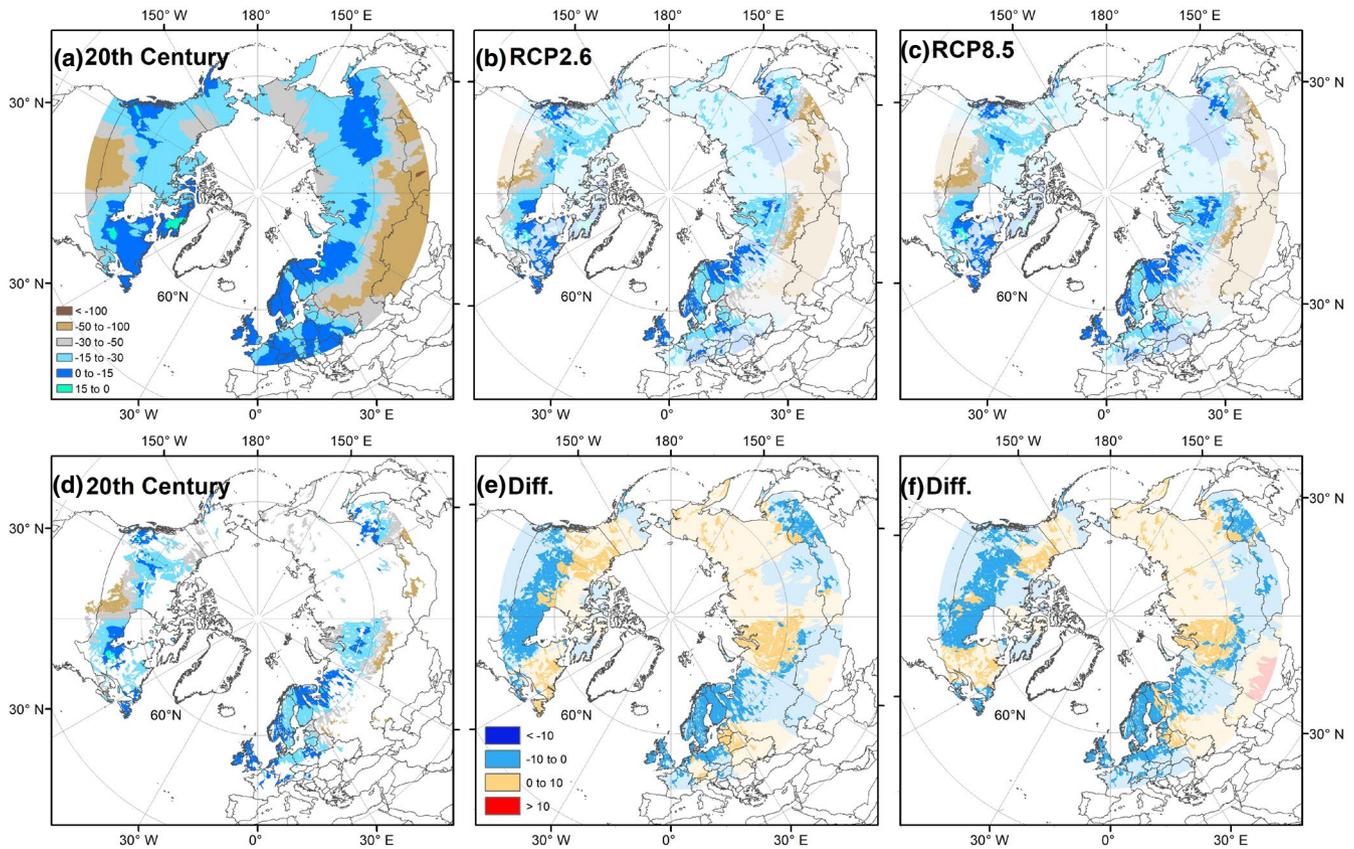
FIGURE 9 Modelled annual water table position (WTP; cm) in the peat soil interpolated among modelled sites averaged over (a) 1991–2000, (b) 2091–2100 for RCP2.6 (Exp26) and (c) 2091–2100 for RCP8.5 (Exp85) scenarios; (d) clipped annual WTP map (average 1990–2000) according to the most up-to-date observed map (PEATMAP; Xu et al. (2018)), difference between RCPs and present day (e) b − a; and (f) c − a

conditions. While the modelled rates are very similar for the two ensembles, the mapped peatland ensemble is used for the upscaling purpose.

We found that northern peatlands have sequestered C at a rate of 20–30 g C m^{-2} year^{-1} since the Holocene with a mean of 21.4 (23.6) g C m^{-2} year^{-1}, largely in agreement with other published long-term records (Loisel et al., 2014; Yu et al., 2009). In the recent past, CARs were in the range of 10–50 g C m^{-2} year^{-1} with a mean of 33.1 (33.9; averaging 1991–2000; Figures 2b,c and 6a,d; Table 1) which on average are higher than the long-term CARs (Figure 3b,c). This is explained by the fact that the recently accumulated peat has not decomposed as much as peat in deeper layers (Yu et al., 2009), in addition to higher CARs due to a warmer climate and higher levels of CO_2 in the atmosphere in the last century. In the coming decades, we find that northern peatlands are likely to continue to act as C sinks under both future climate scenarios. However, their sink capacity is substantially reduced under the high-end climate change scenario (Exp85) after the year 2050 (Figure 3b,c). Compared to present-day CAR estimates of 20–30 g C m^{-2} year^{-1}, the peatland C sequestration capacity will increase until 2050 to 30–35 g C m^{-2} year^{-1}, followed by similar rates as in 2000 for Exp26, while carbon sequestration rates decrease substantially after 2050 for Exp85 (see dotted green and black lines in Figure 3c). Overall, the mean CARs for the 21st century indicate that peatlands will gain comparatively more C under both

warming scenarios (Figure 3b,c). This is in agreement with Gallego-Sala et al. (2018) who also showed a slight increase in the global peatland sink capacity compared to present day until 2100 for both scenarios. Spahni, Joos, Stocker, Steinacher, and Yu (2013) found that northern peatlands will remain a net C sink at least until 2050 AD and a net source afterwards, using a DGVM with nitrogen limitation (LPX—Bern 1.0).

The largest uncertainties arise from insufficiently studied areas, for example, the central and eastern Siberian regions and areas north of 70°N (Loisel et al., 2014), where the true area of peatlands is poorly known. If we assume these areas have a considerable fraction of peat-bearing landscapes, or turn into peatlands due to milder climate conditions and high soil moisture levels, they have the potential to enhance their C sink capacity, thus compensating for some of the projected C loss after 2050 (see Figure 3c). On the other hand, presently permafrost-free areas which experience reduced precipitation rates are likely to experience moisture stress conditions in the future. These areas will lose more C in the near future, particularly peatlands located in the European region and between 45 and 55°N latitude. In Siberia and Europe, only few peatlands are located between 45 and 55°N (see Figure 6d), but a significant fraction of peatland cover in North America falls in this latitudinal zone—Our simulations indicate that these areas may turn into a C source in the near future. Evidence of high C emissions from some of these

low-latitude sites in recent years indicates that they could lose more C in the future (Koehler, Sottocornola, & Kiely, 2011; Roulet et al., 2007). In summary, our findings show that areas in Siberia and north of 70°N have the potential to enhance their C sink capacity, while northern European and North American peatlands (between 45 and 55°N) are most vulnerable to C losses in the coming decades.

All modelled peatlands showed an increase in their plant productivity under the high-warming experiment (Exp85), showing a dominant control of surface air temperature and CO_2 levels on plant productivity and CARs (Figure 4). In the model, shifts in the dominant vegetation distribution occurred between 45 and 55°N and in the Canadian region between 60 and 75°N. Areas dominated by graminoids were found to be diminished in both experiments (Figure 5a–d), implying drier conditions and a deeper WTP (see Figure 9). Drier and warmer conditions in the north promote shrub expansion, affecting plant litter composition and peat (Myers-Smith & Hik, 2018; Vowles & Björk, 2019). In contrast, it is interesting to note that limited warming diminishes soil moisture in the upper layers through evapotranspiration, but is not sufficient to degrade the underlying permafrost and replenish soil moisture. This results in water stress conditions in some areas leading to vegetation damage and stunted growth affecting overall net productivity (Parmentier et al., 2018; Treharne, Bjerke, Tømmervik, Stendardi, & Phoenix, 2019). This issue needs to be explored further to evaluate the impact on productivity in the employed model tools.

The effect of climate change on peatland initiation and expansion is not well understood and currently a topic of active research (Morris et al., 2018). We found that peatland expansion is almost linear since the beginning of the Holocene (Figure 7a), leading to a total area of 3.1 million km^2 occupied by peatlands across the pan-Arctic in by the year 2000 (Xu et al., 2018). Some studies have used different spatial extents in their calculations to compute total C stored in peat-bearing landscapes. Yu et al. (2010) used 4 and 3.7 million km^2, while Gorham (1991), Turunen, Tomppo, Tolonen, and Reinikainen (2002) and Loisel et al. (2014) used a lower value of 3.4 million km^2 in their studies, leading to estimated C pools of 270–674 Pg C in northern peatlands (Yu, Loisel, Charman, Beilman, & Camill, 2014). Since vast areas in eastern and central Russia have not been studied (Loisel et al., 2014), we assume the total peatland area to fall between 3.1 and 4 million km^2 which translates to our estimate of around 500–620 Pg C by the year 2000. The time-history approach makes use of CARs and peatland area change over time to calculate total carbon stocks at each time interval. The carbon stock at each time interval can then be summed up to yield total carbon stocks. If we simply extrapolate the rate of increase in peatland area based on the past changes (see Figure 7), we estimate that around 0.61–0.75 million km^2 could turn to peatlands by the end of this century. Using CARs within the mapped peatland boundary (see Figure 2b), this would mean that peatlands have the potential to take up 9.8–12.5 Pg C under Exp26 or 8.4–10.8 Pg C under Exp85 by the end of 2100. However, both the rate of peatland expansion and the future C sink capacity of peatlands

(Figure 3) are highly uncertain so that these estimates must be regarded with caution.

A recent study by Hodgkins et al. (2018) showed that the near-surface peat in low-latitude peatlands has characteristics similar to the deeper recalcitrant peat layers of northern peatlands. They are characterized by higher aromatic content and low carbohydrates, creating a low oxidation state and higher recalcitrance which is the main reason for their limited mineralization. They concluded that if low-latitude peatlands can withstand an increase of +9°C, northern peatlands might be more resilient to recent and future warming due to similar peat characteristics. This finding highlights the importance of properly constrained peatland PFT characteristics and peat decomposition processes in models, in particular the sensitivity of the deeper, recalcitrant high-latitude peat to recent and projected warming.

5 | CONCLUSION

Our model captured the broad patterns of long-term peatland C dynamics at different spatial and temporal scales while simulating reasonable recent vegetation patterns and permafrost extent across the pan-Arctic region. We used published peat basal ages to constrain peat initiation dates in our model in order to reduce the current and future uncertainties related to peat carbon balance. Under the contrasting emission and warming scenarios RCP2.6 and 8.5, we showed that peatlands on average continue to be carbon sinks in the coming century. However, their sink capacity could be substantially reduced after 2050 under the high-warming scenario due to increases in mineralization rates. Our modelling approach contributes to a better understanding of peatland dynamics and its role in the global climate system at different spatiotemporal scales. A major uncertainty of future predictions is the unknown initiation potential of new peatlands which could potentially change the peatland sink capacity in the future.

Group on Coupled Modelling, which is responsible for CMIP, and we thank the climate modelling groups for producing and making available their model output.

ORCID
Nitin Chaudhary https://orcid.org/0000-0001-7001-3155
Narasinha Shurpali https://orcid.org/0000-0003-1052-4396

REFERENCES
Aerts, R., Verhoeven, J. T. A., & Whigham, D. F. (1999). Plant-mediated controls on nutrient cycling in temperate fens and bogs. *Ecology*, *80*, 2170–2181. https://doi.org/10.1890/0012-9658(1999)080[2170:Pmconc]2.0.Co;2

Alexandrov, G. A., Brovkin, V. A., & Kleinen, T. (2016). The influence of climate on peatland extent in Western Siberia since the Last Glacial Maximum. *Scientific Reports*, *6*. https://doi.org/10.1038/srep24784

Bauer, I. E. (2004). Modelling effects of litter quality and environment on peat accumulation over different time-scales. *Journal of Ecology*, *92*, 661–674. https://doi.org/10.1111/j.0022-0477.2004.00905.x

Chambers, F. M., Booth, R. K., De Vleeschouwer, F., Lamentowicz, M., Le Roux, G., Mauquoy, D., ... van Geel, B. (2012). Development and refinement of proxy-climate indicators from peats. *Quaternary International*, *268*, 21–33. https://doi.org/10.1016/j.quaint.2011.04.039

Chaudhary, N., Miller, P. A., & Smith, B. (2017a). Modelling Holocene peatland dynamics with an individual-based dynamic vegetation model. *Biogeosciences*, *14*, 2571–2596. https://doi.org/10.5194/bg-14-2571-2017

Chaudhary, N., Miller, P. A., & Smith, B. (2017b). Modelling past, present and future peatland carbon accumulation across the pan-Arctic region. *Biogeosciences*, *14*, 4023–4044. https://doi.org/10.5194/bg-14-4023-2017

Collins, W. J., Bellouin, N., Doutriaux-Boucher, M., Gedney, N., Halloran, P., Hinton, T., ... Woodward, S. (2011). Development and evaluation of an Earth-System model-HadGEM2. *Geoscientific Model Development*, *4*, 1051–1075. https://doi.org/10.5194/gmd-4-1051-2011

Cramer, W., Bondeau, A., Woodward, F. I., Prentice, I. C., Betts, R. A., Brovkin, V., ... Young-Molling, C. (2001). Global response of terrestrial ecosystem structure and function to CO_2 and climate change: Results from six dynamic global vegetation models. *Global Change Biology*, *7*, 357–373. https://doi.org/10.1046/j.1365-2486.2001.00383.x

Ekici, A., Chadburn, S., Chaudhary, N., Hajdu, L. H., Marmy, A., Peng, S., ... Beer, C. (2015). Site-level model intercomparison of high latitude and high altitude soil thermal dynamics in tundra and barren landscapes. *Cryosphere*, *9*, 1343–1361. https://doi.org/10.5194/tc-9-1343-2015

French, H. M. (1999). Past and present permafrost as an indicator of climate change. *Polar Research*, *18*, 269–274. https://doi.org/10.3402/polar.v18i2.6584

Friedlingstein, P., Cox, P., Betts, R., Bopp, L., von Bloh, W., Brovkin, V., ... Zeng, N. (2006). Climate-carbon cycle feedback analysis: Results from the C4MIP model intercomparison. *Journal of Climate*, *19*, 3337–3353. https://doi.org/10.1175/JCLI3800.1

Frolking, S., Roulet, N. T., Moore, T. R., Richard, P. J. H., Lavoie, M., & Muller, S. D. (2001). Modeling northern peatland decomposition and peat accumulation. *Ecosystems*, *4*, 479–498. https://doi.org/10.1007/s10021-001-0105-1

Frolking, S., Roulet, N. T., Tuittila, E., Bubier, J. L., Quillet, A., Talbot, J., & Richard, P. J. H. (2010). A new model of Holocene peatland net primary production, decomposition, water balance, and peat accumulation. *Earth System Dynamics*, *1*, 1–21. https://doi.org/10.5194/esd-1-1-2010

Gallego-Sala, A. V., Charman, D. J., Brewer, S., Page, S. E., Prentice, I. C., Friedlingstein, P., ... Zhao, Y. (2018). Latitudinal limits to the predicted increase of the peatland carbon sink with warming. *Nature Climate Change*, *8*, 907–913. https://doi.org/10.1038/s41558-018-0271-1

Gerten, D., Schaphoff, S., Haberlandt, U., Lucht, W., & Sitch, S. (2004). Terrestrial vegetation and water balance – Hydrological evaluation of a dynamic global vegetation model. *Journal of Hydrology*, *286*, 249–270. https://doi.org/10.1016/j.jhydrol.2003.09.029

Gorham, E. (1991). Northern peatlands – Role in the carbon-cycle and probable responses to climatic warming. *Ecological Applications*, *1*, 182–195. https://doi.org/10.2307/1941811

Gorham, E., Lehman, C., Dyke, A., Janssens, J., & Dyke, L. (2007). Temporal and spatial aspects of peatland initiation following deglaciation in North America. *Quaternary Science Reviews*, *26*, 300–311. https://doi.org/10.1016/j.quascirev.2006.08.008

Heinemeyer, A., Croft, S., Garnett, M., Gloor, M., Holden, J., Lomas, M., & Ineson, P. (2010). The MILLENNIA peat cohort model: Predicting past, present and future soil carbon budgets and fluxes under changing climates in peatlands. *Climate Research*, *45*, 207–226. https://doi.org/10.3354/cr00928

Hodgkins, S. B., Richardson, C. J., Dommain, R., Wang, H. J., Glaser, P. H., Verbeke, B., ... Chanton, J. P. (2018). Tropical peatland carbon storage linked to global latitudinal trends in peat recalcitrance. *Nature Communications*, *9*. https://doi.org/10.1038/s41467-018-06050-2

Hugelius, G., Strauss, J., Zubrzycki, S., Harden, J. W., Schuur, E. A. G., Ping, C. L., ... Kuhry, P. (2014). Estimated stocks of circumpolar permafrost carbon with quantified uncertainty ranges and identified data gaps. *Biogeosciences*, *11*, 6573–6593. https://doi.org/10.5194/bg-11-6573-2014

Kleinen, T., Brovkin, V., & Schuldt, R. J. (2012). A dynamic model of wetland extent and peat accumulation: Results for the Holocene. *Biogeosciences*, *9*, 235–248. https://doi.org/10.5194/bg-9-235-2012

Koehler, A. K., Sottocornola, M., & Kiely, G. (2011). How strong is the current carbon sequestration of an Atlantic blanket bog? *Global Change Biology*, *17*, 309–319. https://doi.org/10.1111/j.1365-2486.2010.02180.x

Korhola, A., Ruppel, M., Seppa, H., Valiranta, M., Virtanen, T., & Weckstrom, J. (2010). The importance of northern peatland expansion to the late-Holocene rise of atmospheric methane. *Quaternary Science Reviews*, *29*, 611–617. https://doi.org/10.1016/j.quascirev.2009.12.010

Kuhry, P., & Turunen, J. (2006). The postglacial development of boreal and subarctic peatlands. In R. K. Wieder & D. H. Vitt (Eds.), *Boreal peatland ecosystems* (pp 25–46). Berlin and Heidelberg, Germany: Springer. https://doi.org/10.1007/978-3-540-31913-9_3

Loisel, J., Yu, Z. C., Beilman, D. W., Camill, P., Alm, J., Amesbury, M. J., ... Zhou, W. J. (2014). A database and synthesis of northern peatland soil properties and Holocene carbon and nitrogen accumulation. *Holocene*, *24*, 1028–1042. https://doi.org/10.1177/0959683614538073

MacDonald, G. M., Beilman, D. W., Kremenetski, K. V., Sheng, Y., Smith, L. C., & Velichko, A. A. (2006). Rapid early development of circumarctic peatlands and atmospheric CH_4 and CO_2 variations. *Science*, *314*, 285–288. https://doi.org/10.1126/science.1131722

Malmer, N., Johansson, T., Olsrud, M., & Christensen, T. R. (2005). Vegetation, climatic changes and net carbon sequestration in a North-Scandinavian

subarctic mire over 30 years. *Global Change Biology*, 11, 1895–1909. https://doi.org/10.1111/j.1365-2486.2005.01042.x

McGuire, A. D., Christensen, T. R., Hayes, D., Heroult, A., Euskirchen, E., Kimball, J. S., … Yi, Y. (2012). An assessment of the carbon balance of Arctic tundra: Comparisons among observations, process models, and atmospheric inversions. *Biogeosciences*, 9, 3185–3204. https://doi.org/10.5194/bg-9-3185-2012

Miller, P. A., Giesecke, T., Hickler, T., Bradshaw, R. H. W., Smith, B., Seppa, H., … Sykes, M. T. (2008). Exploring climatic and biotic controls on Holocene vegetation change in Fennoscandia. *Journal of Ecology*, 96, 247–259. https://doi.org/10.1111/j.1365-2745.2007.01342.x

Miller, P. A., & Smith, B. (2012). Modelling tundra vegetation response to recent Arctic warming. *Ambio*, 41, 281–291. https://doi.org/10.1007/s13280-012-0306-1

Mitchell, T. D., & Jones, P. D. (2005). An improved method of constructing a database of monthly climate observations and associated high-resolution grids. *International Journal of Climatology*, 25, 693–712. https://doi.org/10.1002/joc.1181

Morris, P. J., Baird, A. J., & Belyea, L. R. (2012). The DigiBog peatland development model 2: Ecohydrological simulations in 2D. *Ecohydrology*, 5, 256–268. https://doi.org/10.1002/eco.229

Morris, P. J., Swindles, G. T., Valdes, P. J., Ivanovic, R. F., Gregoire, L. J., Smith, M. W., … Bacon, K. L. (2018). Global peatland initiation driven by regionally asynchronous warming. *Proceedings of the National Academy of Sciences of the United States of America*, 115, 4851–4856. https://doi.org/10.1073/pnas.1717838115

Moss, R. H., Edmonds, J. A., Hibbard, K. A., Manning, M. R., Rose, S. K., van Vuuren, D. P., … Wilbanks, T. J. (2010). The next generation of scenarios for climate change research and assessment. *Nature*, 463, 747–756. https://doi.org/10.1038/nature08823

Myers-Smith, I. H., & Hik, D. S. (2018). Climate warming as a driver of tundra shrubline advance. *Journal of Ecology*, 106, 547–560. https://doi.org/10.1111/1365-2745.12817

Obu, J., Westermann, S., Bartsch, A., Berdnikov, N., Christiansen, H. H., Dashtseren, A., … Zou, D. (2019). Northern Hemisphere permafrost map based on TTOP modelling for 2000–2016 at 1 km^2 scale. *Earth-Science Reviews*, 193, 299–316. https://doi.org/10.1016/j.earscirev.2019.04.023

Parmentier, F. J. W., Rasse, D. P., Lund, M., Bjerke, J. W., Drake, B. G., Weldon, S., … Hansen, G. H. (2018). Vulnerability and resilience of the carbon exchange of a subarctic peatland to an extreme winter event. *Environmental Research Letters*, 13. https://doi.org/10.1088/1748-9326/aabff3

Piao, S. L., Sitch, S., Ciais, P., Friedlingstein, P., Peylin, P., Wang, X. H., … Zeng, N. (2013). Evaluation of terrestrial carbon cycle models for their response to climate variability and to CO_2 trends. *Global Change Biology*, 19, 2117–2132. https://doi.org/10.1111/gcb.12187

Pinceloup, N., Poulin, M., Brice, M.-H., & Pellerin, S. (2020). Vegetation changes in temperate ombrotrophic peatlands over a 35 year period. *PLoS ONE*, 15, e0229146. https://doi.org/10.1371/journal.pone.0229146

Ping, C. L., Jastrow, J. D., Jorgenson, M. T., Michaelson, G. J., & Shur, Y. L. (2015). Permafrost soils and carbon cycling. *Soil*, 1, 147–171. https://doi.org/10.5194/soil-1-147-2015

Pope, V. D., Gallani, M. L., Rowntree, P. R., & Stratton, R. A. (2000). The impact of new physical parametrizations in the Hadley Centre climate model: HadAM3. *Climate Dynamics*, 16, 123–146. https://doi.org/10.1007/s003820050009

Qiu, C., Zhu, D., Ciais, P., Guenet, B., Peng, S., Krinner, G., … Hastie, A. (2019). Modelling northern peatland area and carbon dynamics since the Holocene with the ORCHIDEE-PEAT land surface model (SVN r5488). *Geoscientific Model Development*, 12, 2961–2982. https://doi.org/10.5194/gmd-12-2961-2019

Reyes, A. V., & Cooke, C. A. (2011). Northern peatland initiation lagged abrupt increases in deglacial atmospheric CH_4. *Proceedings of the National Academy of Sciences of the United States of America*, 108(12), 4748–4753. https://doi.org/10.1073/pnas.1013270108

Robinson, S. D., & Moore, T. R. (2000). The influence of permafrost and fire upon carbon accumulation in high boreal peatlands, Northwest Territories, Canada. *Arctic Antarctic and Alpine Research*, 32, 155–166. https://doi.org/10.2307/1552447

Roulet, N. T., Lafleur, P. M., Richard, P. J. H., Moore, T. R., Humphreys, E. R., & Bubier, J. (2007). Contemporary carbon balance and late Holocene carbon accumulation in a northern peatland. *Global Change Biology*, 13, 397–411. https://doi.org/10.1111/j.1365-2486.2006.01292.x

Ruppel, M., Valiranta, M., Virtanen, T., & Korhola, A. (2013). Postglacial spatiotemporal peatland initiation and lateral expansion dynamics in North America and northern Europe. *Holocene*, 23, 1596–1606. https://doi.org/10.1177/0959683613499053

Schuldt, R. J., Brovkin, V., Kleinen, T., & Winderlich, J. (2013). Modelling Holocene carbon accumulation and methane emissions of boreal wetlands – An Earth system model approach. *Biogeosciences*, 10, 1659–1674. https://doi.org/10.5194/bg-10-1659-2013

Sitch, S., Huntingford, C., Gedney, N., Levy, P. E., Lomas, M., Piao, S. L., … Woodward, F. I. (2008). Evaluation of the terrestrial carbon cycle, future plant geography and climate-carbon cycle feedbacks using five Dynamic Global Vegetation Models (DGVMs). *Global Change Biology*, 14, 2015–2039. https://doi.org/10.1111/j.1365-2486.2008.01626.x

Smith, B., Prentice, I. C., & Sykes, M. T. (2001). Representation of vegetation dynamics in the modelling of terrestrial ecosystems: Comparing two contrasting approaches within European climate space. *Global Ecology and Biogeography*, 10, 621–637. https://doi.org/10.1046/j.1466-822X.2001.t01-1-00256.x

Smith, B., Warlind, D., Arneth, A., Hickler, T., Leadley, P., Siltberg, J., & Zaehle, S. (2014). Implications of incorporating N cycling and N limitations on primary production in an individual-based dynamic vegetation model. *Biogeosciences*, 11, 2027–2054. https://doi.org/10.5194/bg-11-2027-2014

Spahni, R., Joos, F., Stocker, B. D., Steinacher, M., & Yu, Z. C. (2013). Transient simulations of the carbon and nitrogen dynamics in northern peatlands: From the Last Glacial Maximum to the 21st century. *Climate of the Past*, 9, 1287–1308. https://doi.org/10.5194/cp-9-1287-2013

Stocker, B. D., Spahni, R., & Joos, F. (2014). DYPTOP: A cost-efficient TOPMODEL implementation to simulate sub-grid spatio-temporal dynamics of global wetlands and peatlands. *Geoscientific Model Development*, 7, 3089–3110. https://doi.org/10.5194/gmd-7-3089-2014

Strandberg, G., Kjellström, E., Poska, A., Wagner, S., Gaillard, M.-J., Trondman, A.-K., … Sugita, S. (2014). Regional climate model simulations for Europe at 6 and 0.2 k BP: Sensitivity to changes in anthropogenic deforestation. *Climate of the Past*, 10, 661–680. https://doi.org/10.5194/cp-10-661-2014

Treharne, R., Bjerke, J. W., Tømmervik, H., Stendardi, L., & Phoenix, G. K. (2019). Arctic browning: Impacts of extreme climatic events on heathland ecosystem CO_2 fluxes. *Global Change Biology*, 25, 489–503. https://doi.org/10.1111/gcb.14500

Turunen, J., Tomppo, E., Tolonen, K., & Reinikainen, A. (2002). Estimating carbon accumulation rates of undrained mires in Finland – Application to boreal and subarctic regions. *Holocene*, 12, 69–80. https://doi.org/10.1191/0959683602hl522rp

Vardy, S. R., Warner, B. G., Turunen, J., & Aravena, R. (2000). Carbon accumulation in permafrost peatlands in the Northwest Territories and Nunavut, Canada. *Holocene*, 10, 273–280. https://doi.org/10.1191/095968300671749538

Vowles, T., & Björk, R. G. (2019). Implications of evergreen shrub expansion in the Arctic. *Journal of Ecology*, 107, 650–655. https://doi.org/10.1111/1365-2745.13081

Wania, R., Ross, I., & Prentice, I. C. (2009). Integrating peatlands and permafrost into a dynamic global vegetation model: 1. Evaluation and

sensitivity of physical land surface processes. *Global Biogeochemical Cycles*, 23(3). https://doi.org/10.1029/2008GB003412

Weckstrom, J., Seppa, H., & Korhola, A. (2010). Climatic influence on peatland formation and lateral expansion in sub-arctic Fennoscandia. *Boreas*, 39, 761–769. https://doi.org/10.1111/j.1502-3885.2010.00168.x

Wu, Y. Q., Verseghy, D. L., & Melton, J. R. (2016). Integrating peatlands into the coupled Canadian Land Surface Scheme (CLASS) v3.6 and the Canadian Terrestrial Ecosystem Model (CTEM) v2.0. *Geoscientific Model Development*, 9, 2639–2663. https://doi.org/10.5194/gmd-9-2639-2016

Xu, J. R., Morris, P. J., Liu, J. G., & Holden, J. (2018). PEATMAP: Refining estimates of global peatland distribution based on a meta-analysis. *Catena*, 160, 134–140. https://doi.org/10.1016/j.catena.2017.09.010

Yu, Z. C. (2012). Northern peatland carbon stocks and dynamics: A review. *Biogeosciences*, 9, 4071–4085. https://doi.org/10.5194/bg-9-4071-2012

Yu, Z., Beilman, D. W., & Jones, M. C. (2009). Sensitivity of northern peatland carbon dynamics to Holocene climate change. *Carbon Cycling in Northern Peatlands*. https://doi.org/10.1029/2008GM000822

Yu, Z. C., Loisel, J., Brosseau, D. P., Beilman, D. W., & Hunt, S. J. (2010). Global peatland dynamics since the Last Glacial Maximum. *Geophysical Research Letters*, 37. https://doi.org/10.1029/2010gl043584

Yu, Z. C., Loisel, J., Charman, D. J., Beilman, D. W., & Camill, P. (2014). Holocene peatland carbon dynamics in the circum-Arctic region: An introduction. *Holocene*, 24, 1021–1027. https://doi.org/10.1177/0959683614540730

Zhang, W., Jansson, C., Miller, P. A., Smith, B., & Samuelsson, P. (2014). Biogeophysical feedbacks enhance the Arctic terrestrial carbon sink in regional Earth system dynamics. *Biogeosciences*, 11, 5503–5519. https://doi.org/10.5194/bg-11-5503-2014

SUPPORTING INFORMATION

Additional supporting information may be found online in the Supporting Information section.

How to cite this article: Chaudhary N, Westermann S, Lamba S, et al. Modelling past and future peatland carbon dynamics across the pan-Arctic. *Glob Change Biol*. 2020;26:4119–4133. https://doi.org/10.1111/gcb.15099